

Structural and Elastic Properties of Chromium Substituted Nickel Ferrites

V. T. Muttannavar¹, Pradeep Chavan², Geeta Chavan³, P. B. Belavi⁴ and L. R. Naik²

¹Department of Physics, J. S. S. College, Dharwad, Karnataka, India – 580 003

²Department of Physics, Karnatak University, Dharwad, Karnataka, India – 580 003

³Department of Physics, Karnataka Science College, Dharwad, Karnataka, India – 580 003

²Department of Physics, Gogte Institute of Technology, Belgaum, Karnataka, India – 590 008

Email: naik_40@rediffmail.com

Abstract

Polycrystalline ferrites with general formula $Cr_xNi_{1-x}Fe_2O_4$, (in which $x = 0.0$ to 0.4) were synthesized by conventional solid state reaction method. The structural parameters such as crystallite size, lattice constant, miller indices, interplanar distance and porosity were estimated using X-ray diffraction measurement. The existence of single phase cubic spinel structure of ferrites without impurities was confirmed by XRD measurement. The crystallite size increases with increase in bismuth concentration (ranging from 283nm to 528nm). The lattice constant increases with increase of bismuth content. IR absorption bands observed at $410cm^{-1}$ and $590cm^{-1}$ confirm the existence of octahedral and tetrahedral complexes. The elastic parameters of Bismuth substituted Ni-Cu ferrites such as longitudinal elastic wave velocity, transverse elastic wave velocity, modulus of rigidity, young's modulus, and bulk modulus and Debye temperature were estimated by using FTIR study. Debye temperature was found to decrease from $463^{\circ}C$ to $425^{\circ}C$ as the concentration of bismuth increases. The oxygen positional parameter (σ) obtained at around 0.35 was due to the strengthening of inter atomic bonding between various atoms continuously.

Keywords: Sintering, XRD, FTIR, Elastic parameters, Debye temperature.

1. Introduction

The study of polycrystalline ferrites have been carried out from several years due to their wide range of applications as magnetic materials. The interest in these oxides emerges from their versatile applicability in telecommunication, audio and video, power transformers and many other applications involving electrical signals normally not exceeding a few megacycles per second (Rosales et al. 1995). The materials which have high magnetization and less energy loss with high frequency are most frequently applicable for electronic devices. Among such materials, Nickel ferrites are more applicable in electronic technology because they have high electrical resistivity, low eddy currents loss and appropriate dielectric loss (Bammannavar et al. 2008). Recently, the surface mount devices (SMD) technology has been rapidly developed for miniaturation of electronic devices such as a multilayer ferrite chip inductors. The multilayer ferrite chip inductors are produced by coating ferrite and electrode layers alternatively and co-firing those (Chavan et al. 2017). These ferrimagnetic materials belong to wide group of spinel compounds having a general formula AB_2O_4 (Chavan et al. 2018). X-ray diffraction measurement can provide important information regarding structural properties of ferrites. The angle of diffraction and intensity of diffracted beam together are the characteristics of particular crystal structure, since no two atoms have exactly the same size and X-ray scattering ability; the intensities of the diffracted beam will be unique for every materials. This uniqueness helps to identify the structure and estimation of structural parameters of the materials (Bhatu et al. 2007). In most of the ferrite materials, the substituent's play an important role in

determining the variation of physical properties. Nickel ferrite is the most suitable in which the magnetic and transport properties are affected by the substituent (Roy et al. 2008).

In the present study, solid state reaction method is used for the preparation of ferrites. The study of structural and elastic properties of ferrites has been carried out in this work.

2. Experimental Details

The ferrite materials with the general formula $\text{Cr}_x\text{Ni}_{1-x}\text{Fe}_2\text{O}_4$ (with $x = 0.0, 0.1, 0.2, 0.3$ and 0.4) were synthesized by solid state reaction method. The materials used for the synthesis of ferrites are high purity AR grade metal oxides. By keeping the stoichiometry balanced, CrO_2 , NiO and Fe_2O_3 powders were mixed in acetone medium and grounded until the acetone evaporates and becomes homogeneous mixture of the metals. The fine powder was grounded for longer duration to reduce the particle size. The fine powder mixture was presintered at 800°C for 8 hrs in a muffle furnace and then cooled to room temperature. This presintered powder was pressed into the form of pellets. These pellets were final sintered at 1150°C for 12 hrs and cooled to room temperature. The final sintered pellets were crushed into the agate mortar to get the fine powder with less particle size which is further used for the study of confirmation of cubic spinel structure of ferrite using XRD technique (Philips Model PW-1710) with $\text{Cu-K}\alpha$ radiation ($\lambda = 1.5406\text{\AA}$). The IR absorption bands were studied using FTIR spectroscopy and the elastic properties were discussed with the help of FTIR spectrographs (model: NICOLET 6700). The Atomic Force Microscope (AFM) technique is used to scan the specimen surface in a raster pattern with the help of commercial silicon probe (Nanosurf Easyscan2).

3. Result and Discussion

Figure.1 shows the XRD pattern of Cr substituted Ni ferrites. All the peaks appeared in the XRD pattern are indexed with the help of JCPDS data's, non-observation of extra peaks confirmed the formation of single phase cubic spinel structure of ferrites without impurities. The peaks with the (h k l) values of (111), (220), (311), (222), (400), (422), (511), (440), (620), (533), and (444) shows the characteristics of the single phase cubic spinel structure of the ferrites (Chavan et al. 2017). From figure 1, it is observed that the decrease of lattice constant with increase of the concentration of Cr in Nickel ferrites was due to the replacement of Cr ions with Fe^{3+} ions and also due to the difference of ionic radius in the ferrites (Bahgat et al. 2008), (Belavi et al. 2012). Since the ionic radius of Fe^{3+} is (0.645\AA), the ionic radius of Cr^{2+} (0.52\AA), Ni^{2+} ions has the ionic radius of (0.69\AA); hence the lattice constant found to decrease. It is also observed that as the concentration of Cr^{2+} increases in the ferrites, the intensity of diffraction peaks increases; it was due to the variation in crystallite size and ionic radii of the metal ions.

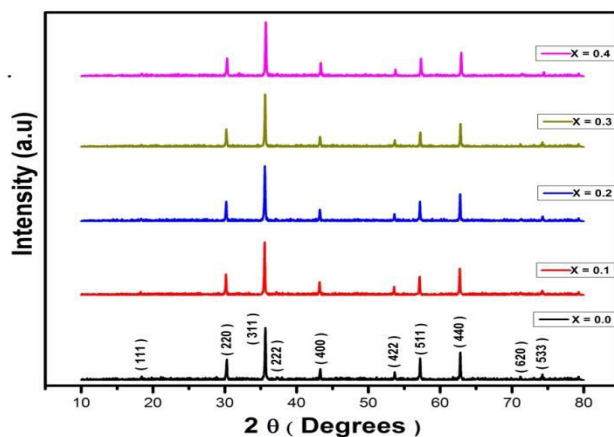


Fig.1 XRD graphs of $\text{Cr}_x\text{Ni}_{1-x}\text{Fe}_2\text{O}_4$ ferrites (x varies from 0.0 to 0.4).

The addition of Cr in Nickel ferrites shows the grain growth as evident from X-ray diffraction pattern. From the X-ray diffraction pattern, the crystallite size was estimated by using Scherer formula which is found to be increases with increasing the concentration of Cr ions (ranges from 283 nm to 528 nm).

4. FTIR Studies

In ferrite, the metal cations are situated in two different sub-lattices, namely tetrahedral (A-sites) and octahedral (B-sites) sites according to the geometric configuration of the oxygen ion nearest neighbor atoms. According to Waldron (Waldron et al. 1955) and Hafner (Hafner et al. 1961), the IR absorption bands observed at 600 cm^{-1} and 400 cm^{-1} corresponds to the stretching vibrations of tetrahedral (ν_1) and octahedral group (ν_2). In all ferrite samples, it is observed that the two prominent absorption bands ν_1 (580 cm^{-1}) and ν_2 (403 cm^{-1}) corresponds to the tetrahedral and octahedral sites (A-site and B-site) respectively shown in the figure.2. A very weak ν_3 band (471 cm^{-1}) is also observed when the concentration of Cr increases in Nickel ferrites (Patange et al., 2013). Thus the appearance of ν_3 band in IR spectra of Nickel ferrites was due to the divalent metal ion oxygen complexes in octahedral site. The absorption bands for Cr substituted Nickel ferrites found to be in expected range. These absorption bands are the common features of cubic spinel ferrites and confirmed the structural formation of the ferrite system. The positions of ν_1 and ν_2 bands are in expected range due to the differences in the $\text{Fe}^{3+}\text{-O}^{2-}$ distances for A-B site. The presence of Fe^{2+} ions causes the splitting of absorption bands due to local lattice deformation caused by Jahn-Teller effect (Bhosale et al. 2006).

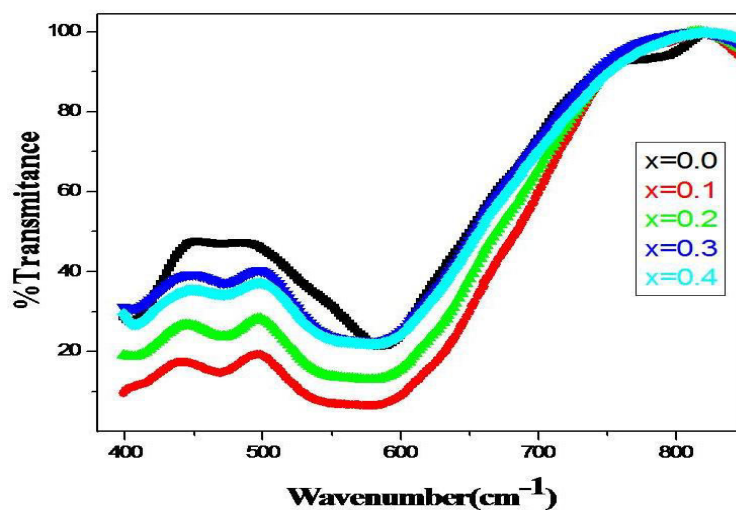


Fig.2 IR absorption spectrum of Cr substituted Nickel ferrites.

5. Atomic Force Microscope (AFM)

Figure 3 shows the AFM images of Cr substituted Nickel ferrites. For each sample, the crystallite size was measured directly on AFM images taken. The average crystallite size estimated was 217 nm (ranges from 173 nm to 263 nm). In AFM micrograph, the grains are well crystallized, very dense, and quite smooth (Tong et al. 2011). If the grains are dispersed on the specimen surface, lateral interaction between the tip and the grains distorted the shape of the crystallites and increases their grain size (Shaikh et al. 1999). If the crystallite size were closely packed i.e. if they touch one another, interaction with the probe occurs mainly at the top of the grains, so that actual crystallite size should be adequately measured.

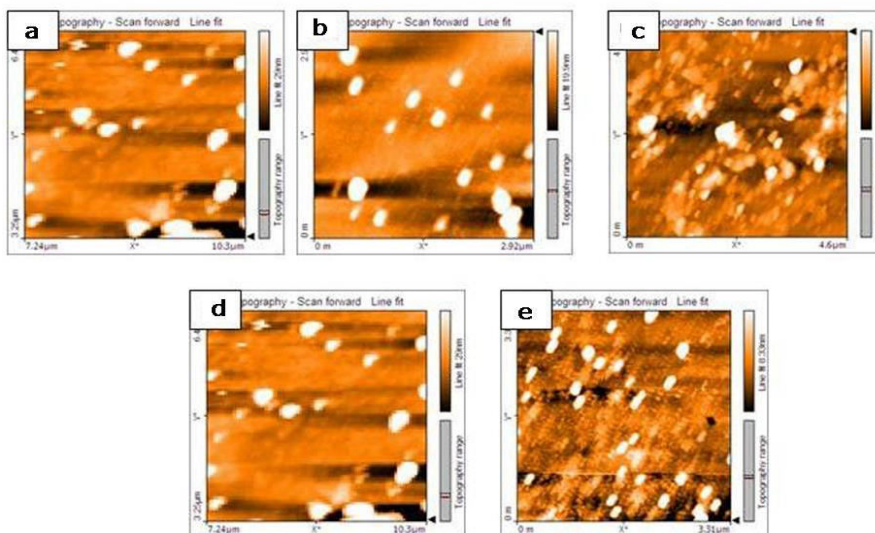


Fig.3 AFM images of Cr substituted Nickel ferrites.

6. Elastic Properties

The constants of elasticity are of much importance in studying the ferrites, the elastic constants expresses the behavior of binding forces in solid materials and helps to understand the thermal properties of the solid materials. The IR absorption bands of Cr^{2+} substituted Nickel ferrites are listed in table.1. The force constants of tetrahedral and octahedral sites (K_t and K_o) and the other parameters such as the ionic radii of A and B-sites (r_A and r_B), theoretical lattice constant (a_0), oxygen positional parameter (u), tetrahedral bond length (d_{AL}), octahedral bond length (d_{BL}), tetrahedral edge length (d_{AE}), octahedral edge length (d_{BE}), unshared octahedral edge length (d_{BEU}), jump lengths of A and B-sites (L_A and L_B) and the elastic constants such as bulk modulus (B), modulus of rigidity (G), young's modulus (E), poisons ratio (σ), longitudinal elastic wave velocity (V_l), transverse elastic wave velocity (V_s), mean elastic wave velocity (V_m) and debye temperature (θ) (Belavi et al. 2012) estimated in our study are listed in table.1 (Modi et al. 2006), (Chavan et al. 2018).

Table 1. Structural and Elastic parameters of Cr substituted Nickel ferrites.

Parameters	X=0.0	X=0.1	X=0.2	X=0.3	X=0.4
a_0 (Å)	8.356	8.356	8.346	8.335	8.334
$\rho \times 10^3$ (kg/m ³)	5.388	6.085	6.807	7.536	8.242
a_t (Å)	8.302	8.339	8.376	8.414	8.451
r_A (Å)	0.74	0.807	0.874	0.941	1.008
r_B (Å)	1.34	1.302	1.264	1.226	1.188
u	0.403	0.408	0.412	0.417	0.422
d_{AL}	2.218	2.286	2.353	2.419	2.487
d_{BL}	1.881	1.851	1.824	1.797	1.777
d_{AE}	3.623	3.753	3.843	3.951	4.061
d_{BE}	2.285	2.174	2.058	1.942	1.831
d_{BEU}	2.991	3.004	3.017	3.030	3.049

L_A	3.618	3.618	3.613	3.609	3.609
L_B	2.954	2.954	2.950	2.947	2.946
$v_1 \times 10^2 (m^{-1})$	403	403	403	403	407
$v_2 \times 10^2 (m^{-1})$	586	580	579	580	580
$K_t (N/m)$	1.629	1.631	1.632	1.633	1.637
$K_o (N/m)$	3.450	3.381	3.370	3.383	3.384
$B \times 10^9 (kgm^{-1}s^{-2})$	108.9	108.6	108.4	108.3	108.4
$V_1 (m/s)$	4496	4225	3991	3791	3627
$V_s (m/s)$	2595	2439	2304	2188	2094
$G \times 10^9 (kgm^{-1}s^{-2})$	36.28	36.19	36.13	36.07	36.13
σ	0.35	0.35	0.35	0.35	0.35
$E \times 10^9 (kgm^{-1}s^{-2})$	97.96	97.77	97.55	97.39	97.55
$V_m (m/s)$	2373	2230	2106	2000	1893
$\theta (^{\circ}K)$	463	452	442	433	425

These estimated parameters are in good agreement with the values reported earlier. The Poisson's ratio (σ) is found to be 0.35 for each concentration of samples, which lies in the range from -1 to 0.5 and it confirms the theory of isotropic elasticity (Chavan et al. 2017). The oxygen positional parameter (u) is found to increase with increasing the concentration of Cr. The decrease of elastic parameters with increase in the concentration of Cr was due to the strengthening of inter atomic bonding between various atoms continuously.

7. Conclusions

The solid state reaction method was used to synthesize the Cr substituted Nickel ferrites. Structural analysis with powder XRD reveals the formation of a single phase cubic spinel structure of Cr^{2+} substituted Nickel ferrites. Tetrahedral elastic parameters are found to increase whereas octahedral parameters are found to decrease with increase of Cr^{2+} concentration in the ferrites. The elastic parameter studied shows the nature of binding forces in polycrystalline materials. The Poisson's ratio (σ) is found to be 0.35 for each concentration of samples which lies in the range from -1 to 0.5 and it confirms the theory of isotropic elasticity.

Acknowledgement

The authors thank to the Director and technical staff of University Science Instrumentation Center (USIC), Karnatak university, Dharwad for their support during FTIR and AFM measurement.

References

1. Rosales, M. I., Plata, A. M., Nicho, M. E., Brito, A., Ponce, M. A., Castano, V. M., 1995; J. Mater. Sci. 30, 4446.
2. Bammannavar, B. K., L. R. Naik, & R. B. Pujar, 2008; J. Mater. Sci & Engg. 4(3), 160.
3. Kim, W.C., S. J. Kim, S. W. Lee, C. S. Kim, 2001; J. Magn. Magn. Mater. 226, 1418.
4. Chavan, P., L. R. Naik & R. K. Kotnala, 2017; J. Magn. Magn. Mater. 433, 24.



5. Modi, K. B., M. K. Rangolia, M. C. Chhantbar, H. H. Joshi, 2006; J. Mater Sci, 41, 7308.
6. Chavan, P. and L. R. Naik, 2018; Vacuum. 152 , 47.
7. BHATU et al. 2007; Indian journal of pure and applied physics 45, 596.
8. Roy, P. K., Bibhuti B. Nayak, J. Bera, 2008; J. Magn. Magn. Mater. 320, 1128.
9. Chavan, P., L.R. Naik, P.B. Belavi, Geeta Chavan and R.K. Kotnala, 2017; J. Alloys. Compds. 694, 607.
10. Bahgat, M., M. K. Paek and J., 2008; J. Pak Mater. Transactions, 49(4), 860.
11. Belavi. P. B. et al., 2012; Mater. Chem. Phy. 132, 138.
12. Waldron, R. D., 1955; Phys. Rev. 99, 1727.
13. Hafner, S. T. Z., 1961; Kristallogr. 115, 331.
14. Patange, S.M. et al., 2013; J. Molecular. Struct. 40, 1038.
15. Bhosale, A.G., B.K. Chougule, 2006; Mat. Chem. and Phys. 97, 273.
16. Tong, J. J. et al, 2011; Vacuum 86, 340.
17. Shaikh, A.M. et al., 1999; J. Magn. Magn. Mater. 195, 384.
18. Chavan, P. and L. R. Naik, 2017; Physica. Status. Solidi. A. 1700077, 1.